Molecular approach to the interpretation of the dielectric relaxation spectrum of a molecular glass former

M. A. González
Institut Laue Langevin, Boîte Postale 156, F-38042 Grenoble Cedex 9, France

E. Enciso
Departamento de Química Física I, Facultad de Ciencias Químicas, Universidad Complutense, Madrid E-28040, Spain

F. J. Bermejo and M. Jiménez-Ruiz
Consejo Superior de Investigaciones Científicas, Serrano 123, Madrid E-28006, Spain

M. Bée
Laboratoire de Spectrométrie Physique, UMR 5588, Université J Fourier Grenoble-I, Boîte Postale 87, Domaine Universitaire, F-38402, Saint-Martin d'Hères Cédex, France

(Received 9 November 1999)

The frequency-dependent dielectric function of ethanol at temperatures within the normal liquid range is evaluated by means of computer molecular dynamics simulations and compared with recent experimental data. The calculated spectra show a similar structure to those reported from experimental measurements and the temperature dependence of its most prominent bands also follows the experimental estimates. An attempt is also made to assign the most intense bands to specific molecular reorientations.

PACS number(s): 61.20.Lc, 02.70.Ns, 77.22.Gm

I. INTRODUCTION

The interest in understanding the microscopic origin of the most prominent features appearing in the dielectric function $\epsilon(\omega)$ of low-molecular-weight glass-forming liquids stems for the wide use of the technique as a tool for exploring the dynamics of very viscous (supercooled) liquids over many frequency decades [1]. In this respect, the dynamics of most molecular materials as explored by dielectric spectroscopy shows a rather characteristic behavior as the glass-transition temperature T_g is approached from above. While the usual Vogel-Fulcher-Tamann (VFT) equation

$$\tau(T) = \tau_0 \exp[A/(T - T_0)] \tag{1}$$

is followed by the dielectric relaxation time $\tau(T)$ down to T_g, a limiting temperature T_A seems to exist in low molecular-weight liquids [2,3] above which the behavior of $\tau(T)$ is better described by a simple Arrhenius law.

In contrast with polymers and complicated organics, the study of low-molecular-weight glass forming liquids opens up the possibility of understanding the dynamics about the glass transition without having to recourse to strong assumptions concerning the nature of motions being sampled within a given experimental frequency window. A number of materials has been investigated in recent times and some common trends have been found [3,4]. Among them, liquid ethanol has been investigated using a full suite of techniques such as dielectric relaxation [5–7], far-infrared spectroscopy [8], NMR relaxation [9–14], viscosity measurements [7,14], light scattering [14], or incoherent quasielastic neutron scattering [14]. The picture that emerges out of such studies is not fully consistent, due perhaps to a number of asumptions employed when analyzing the data.

In addition, the material has been thoroughly investigated recently in connection with the glass transition [15–17]. As known since two decades ago [18], ethanol can be quenched avoiding crystallization to form a glass which shows a glass transition temperature $T_g = 97$ K. If the liquid is cooled down at a rate about 2 K/min or the glass is annealed between 97 and 115 K, a rotator-phase (RP) crystal is formed, where the molecules are translationally ordered on a bcc lattice but can rotate freely. Dynamically, such phase has been shown to be remarkably close to the supercooled liquid (SCL) at least at the characteristic scales sampled in dielectric relaxation experiments [4]. This phase also undergoes a further calorimetric glass transition at about 97 K, involving the freezing of the molecules at random orientations, leading to an orientational glass.

The similitude in relaxational behavior of the SCL and RP phases thus provides some clues on the importance of reorientational motions at temperatures about T_g but it still does not tell much about the microscopic origin of both relaxations as sampled in dielectric experiments [4,19]. Our aim here is therefore to contribute towards the understanding of the dielectric spectrum of ethanol at temperatures above T_A, that is in the low-viscosity regime, where most motions are expected to show a dominant single-particle character. For us this seems to be a prerequisite for the understanding of the far more complex dynamics of the supercooled liquid which shows charateristic relaxations beyond reach of the current computing capabilities. To achieve the above stated aim we explore by means of molecular dynamics (MD) simulations the reorientational motions and the dielectric behavior of a simple model of ethanol. The performance of the employed force field as well as some alternatives for its possible improvement were described in a previous contribution [20], as it also were the predicted features concerning some dynami-

TABLE I. Simulated thermodynamic states and results obtained for the static dielectric constant $\epsilon(0)$ and the single and collective relaxation times in ps (see text). The experimental results for $\epsilon(0)_{expt}$ have been taken from Refs. [45] (at 273 K), [6] (at 298 K), and [46] (between 333 and 500 K).

Run	T (K)	ρ (g/cm^3)	Simulation time (ns)	$\epsilon(0)$	$\epsilon(0)_{expt}$	τ_1^{col} (ps)	τ_2^{col} (ps)	τ_1^{self} (ps)	τ_2^{self} (ps)
A	273	0.806	8.2	20 ± 3	28.5	155	3.4	49	12 (1 .5,16)
B1	298	0.785	4.9	18 ± 3	24.3	67	1.2	39	8.1 (1.1,11)
B2	300	0.785	6.0	19 ± 3	24.3	62	1.5		
B3[a]	300	0.785	2.0	17 ± 5	24.3	104	13		
B4[b]	294	0.785	2.0	19 ± 5	24.3	72	2.0		
C	333	0.754	4.9	11.6 ± 0.6	19.7	19	0.93	15	2 .1 (0.65,4.1)
D	353	0.737	4.9	11.5 ± 0.4	17.2	13	0.37	10	1 .8 (0.61,3.5)
E1	400	0.681	4.9	8.6 ± 0.2	12.6[d], 10.6[e]	5.4	0.54	4.4	1.0
E2[c]	400	0.681	2.0	9.1 ± 0.4	12.6[d], 10.6[e]	4.9	0.46		
F	450	0.605	4.9	6.3 ± 0.2	7.5[f]	2.9	0.84	2.2	0.54
G	500	0.469	4.9	4.1 ± 0.1	4.4[g]	1.4	0.27	1.2	0.44

[a]With 524 molecules.
[b]With 524 molecules and $R_s=17$ Å, $R_c=18$ Å.
[c]With $\epsilon_{rf}=8.6$.
[d]At 393 K.
[e]At 413 K.
[f]At 453 K.
[g]At 503 K.

cal aspects of the normal and supercooled liquids [21]. Explicitly, here we investigate the origin of the three distinct relaxations found in dielectric measurements on liquid primary alcohols [5,6], which still needs clarification.

II. MODEL AND COMPUTATIONAL DETAILS

MD simulations at seven different temperatures have been carried out using the OPLS potential [22], which gives good results for the main thermodynamic and dynamic properties of liquid and glassy ethanol. The simulated system consisted of 216 ethanol molecules placed in a cubic box with periodic boundary conditions. All the simulations were performed in the microcanonical ensemble (constant NVE) at the experimental densities [23]. The equations of motion were integrated using the Verlet leap-frog algorithm [24] with a time step of 2.5 fs and bond lengths and angles were constrained by means of the SHAKE algorithm [25]. The interparticle interactions were truncated using a cutoff $R_c=12.5$ Å and a switch function to avoid energy drifts [26]. The chosen form was that described by Alonso *et al.* [27], and as before we used $R_s=11.5$ Å, being R_s the onset of the switching function [20]. Long-range corrections due to the neglect of dispersion interactions beyond R_c were applied [24] and the electrostatics was treated using the reaction field technique with a constant $\epsilon_{rf}=25$ for the dielectric permittivity of the continuum [24,28]. This value comes close to the experimental static dielectric constant of ethanol at ambient temperature [6] and we used the same constant in all the simulations performed. This method of treatment of the long-range interactions has proven to give results that agree with those obtained using Ewald sums [29,30] and is simpler and faster than the later. In contrast, the results are more size-dependent than those obtained when using lattice methods, so some care needs to be exercised. In consequence, we checked the validity of our results in different ways, as it is detailed below.

III. RESULTS

A. Statistical accuracy and size effects

To check the statistical accuracy of our data as well as boundary conditions and size effects, we performed several tests. Four different runs (B1–B4) were carried out for room temperature conditions. Runs B1 and B2 were carried under exactly the same conditions, which are those described in the previous section and employed in all the other runs at different temperatures. This provides some measure for estimating the error bars of the calculated data as well as the maximum time at which the collective correlation functions studied here are obtained with reasonable accuracy. In run B3 we simulated a larger system, with 524 molecules instead of 216, but with the same cutoff than that used previously, while in run B4 we employed again 524 molecules and a longer cutoff, $R_s=17$ Å and $R_c=18$ Å. This allows us to test independently the effects of increasing the size of the system or the cutoff employed. Three properties have been considered in some detail: the static dielectric constant, the total dipole time autocorrelation function and the distance dependent Kirkwood factor.

The static dielectric constant $\epsilon(0)$ was calculated using the appropriate formula for the reaction field boundary conditions [31]

$$\frac{1}{4\pi\varepsilon_0}\frac{4\pi}{3}\frac{\langle \boldsymbol{M}^2\rangle}{3Vk_BT}=\frac{[\epsilon(0)-1][2\epsilon_{rf}+1]}{3[2\epsilon_{rf}+\epsilon(0)]}, \qquad (2)$$

where ε_0 is the vacuum permittivity, $\boldsymbol{M}=\Sigma_i\boldsymbol{\mu}_i(t)$ is the total dipole moment of the system, V is the volume, and T is the average temperature. The results of the four runs are given in

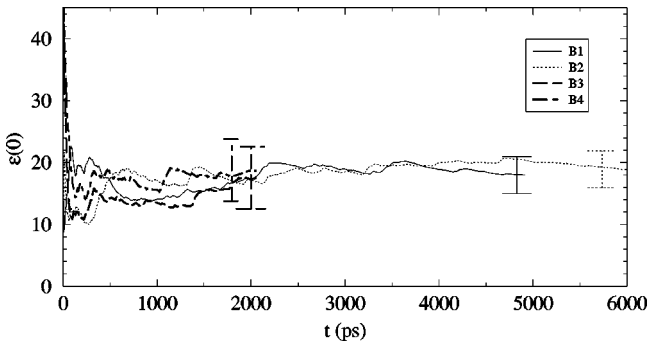

FIG. 1. Running average of the static dielectric constant at 298 K using different conditions (see text for details).

Table I. They agree within their statistical error [32] and they are also in agreement with the value of $\epsilon(0)=16\pm1$ obtained using the Ewald sum method [33]. The running average for this quantity along the simulation is plotted in Fig. 1, which clearly shows that very long times are required in order to achieve convergence of this property and reduce the error bars down to acceptable sizes

The total dipole time autocorrelation function

$$\Phi(t)=\frac{\langle \boldsymbol{M}(0)\boldsymbol{M}(t)\rangle}{\langle \boldsymbol{M}^2\rangle}, \tag{3}$$

is shown in Fig. 2. The curves corresponding to runs B1 and B2 agree reasonably well up to 50–60 ps, while the other two show deviations due to the larger error incurred when performing shorter runs. Taking into account the large error bars shown in the figure, one sees that the calculated relaxation times obtained from fits of the curves to a biexponential function (see next subsection and Table I) are also in good agreement with those reported for the Ewald method [33]. This figure also illustrates the difficulties involved in the calculation of dielectric properties, and in particular, it shows how accurate values for the computation of $\Phi(t)$ are in this case only those up to a maximum time of about 50–60 ps, i.e., about one hundredth of the total simulation time.

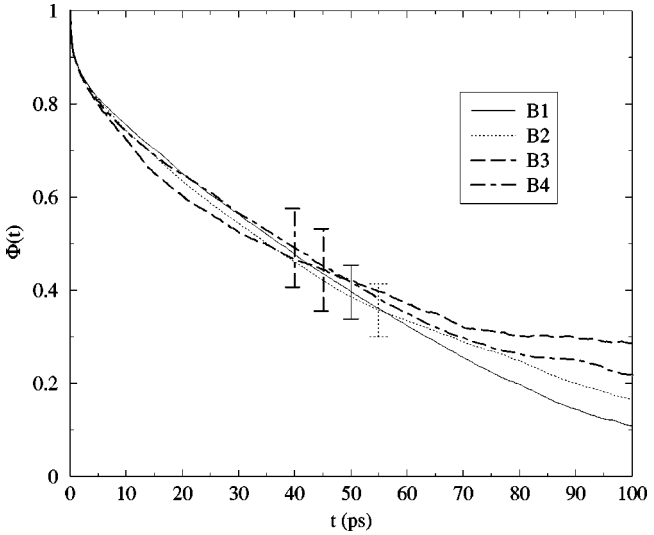

FIG. 2. Total dipole time autocorrelation function at 298 K using different conditions (see text for details).

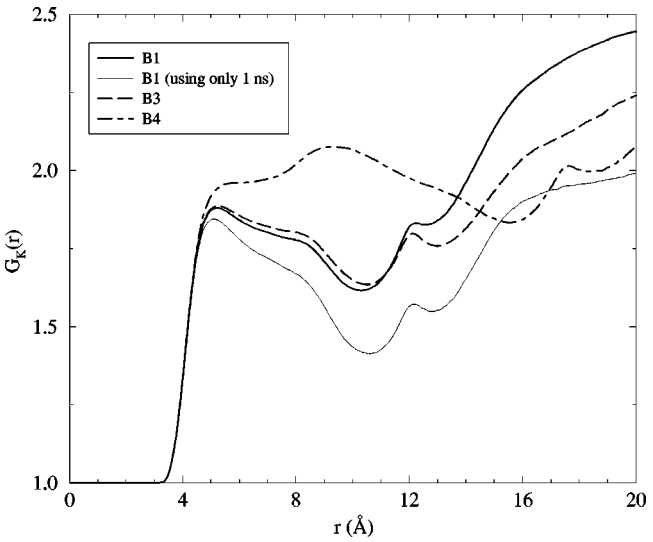

FIG. 3. Distance dependent Kirkwood factor using different conditions (see text for details).

The distance-dependent Kirkwood factor

$$G_K(r)=\frac{1}{N}\left\langle \frac{1}{\mu^2}\sum_i \sum_{j,r_{ij}<r} \boldsymbol{\mu}_i\boldsymbol{\mu}_j \right\rangle \tag{4}$$

has also been evaluated and it is shown in Fig. 3. Once again, large errors are involved, as can easily be checked by comparing the two curves corresponding to run B1, one of them calculated averaging over the full trajectory and the other computed averaging only over the first nanosecond of simulation, which is the same time used for the calculation of $G_K(r)$ for runs B3 and B4. These quantities have been evaluated using the whole of the simulation box, so some artifacts could appear due to the use of the minimum image convention for distances beyond $L/2$, corresponding to the radius of the largest sphere that is containable into the simulation box [30]. This radius is 13.8 Å for run B1, and 18.5 Å for runs B3 and B4, but no important distortions are apparent in our results due to this fact, as checked by comparing the curves corresponding to runs B1 and B3. Thus, the use of a larger system does not modify much the dipole-dipole correlations. However, the use of a longer cutoff do change greatly the behavior of $G_K(r)$, shifting and increasing the height of the second peak and moving the first minimum and the following maximum to distances close to the new cutoff. Therefore, this feature seems to be directly related to the cutoff of long range interactions.

An extensive study about the use of the reaction field method and the influence of the conditions employed has been done by Van der Spoel *et al.* for the case of water [34]. They found that $\epsilon(0)$ increased when using a larger system, while there were no clear systematic effects on the dielectric behavior when a longer cutoff was used, although large differences in $G_K(r)$ appear [34]. The errors of our data prevent a full confirmation of their conclusions, but it seems that in our case size effects, if any, are of little importance in comparison with the statistical errors incurred in the calculation of collective properties, unless extremely long simulations are carried out. As an example, we find that our simulations of 2 ns carried out using a larger system are still too short to

allow a clear comparison with the longer runs, as Figs. 1 and 2 clearly evidence. However, the agreement between the results presented here and those found using the Ewald method [33] indicates that in this case the particular boundary conditions employed do not change significantly the static dielectric constant nor the total dipole time autocorrelation function. Nevertheless, as far as the distance-dependent Kirkwood factor is concerned, our data clearly confirm the observations of Ref. [34], indicating that long range dipole-dipole correlations indeed are dependent upon the particular conditions employed. Further studies to check the extent of these effects and the best way to eliminate them are required.

Finally, we have also checked the influence of the used reaction field constant. As indicated in the previous section, we have always used $\epsilon_{rf}=25$, which corresponds roughly to the experimental dielectric constant of ethanol at normal conditions. At 298 K this is about 30% higher than the dielectric constant corresponding to the model employed (see Table I) and such difference increases with increasing temperature. Since that constant appears in the reaction field method only in the expression $2(\epsilon_{rf}-1)/(2\epsilon_{rf}+1)$, which goes rapidly to one with increasing ϵ_{rf}, the results are quite insensitive to the particular choice [24]. Nevertheless, we decided to test which was the effect of replacing it by the lower value corresponding to the real dielectric constant of the model, so at 400 K we performed a second simulation using the dielectric constant obtained in the first run. The results obtained for the dielectric constant and the collective relaxation times are shown in Table I. The differences between both runs are quite small, thus indicating that the use of the same reaction field constant at all temperatures does not largely affect our results.

As a whole, all these aspects evidence the problems found when calculating dielectric properties and the magnitude of the errors involved. However, the similarity of the results obtained in runs B1 and B2 indicates that the simulations performed are long enough to allow us to obtain reliable data for the dielectric constant and the total dipole time autocorrelation function, although for the later only the initial part of the curve is obtained with reasonable accuracy.

When comparing with experiment, the agreement is only qualitative, as the results obtained for the dielectric constant or the dielectric correlation times are considerably smaller than those found experimentally. The same has been observed for methanol [35,36]. For water, a great number of different models have been used in order to reproduce different experimental results and they show different degrees of success in what refers to dielectric properties, but it seems, however, that no simple model is able to account quantitatively for the whole of empirical observations (see, e.g., Refs. [34,37], and references therein). Even more complex models, where polarization is introduced explicitly and not through the use of an effective dipole moment, do not improve the agreement between simulation and experiment in this aspect [38]. Nevertheless, this drawback does not put into question the usefulness of our simulations, as the qualitative or, for some properties, even quantitative agreement gives confidence in that the basic physics is well accounted for, so that the information yielded by the simulations can be used to understand better which microscopic processes give rise to the experimental observations.

B. Static dielectric constant

The static dielectric constant was calculated by means of Eq. (2) and the results obtained for each temperature are shown in Table I. The calculated $\epsilon(0)$ is consistently below experiment at all temperatures, although such discrepancy becomes less important with increasing temperature.

Using a model very similar to that employed here, Skaf *et al.* [36] obtained $\epsilon(0)=24\pm2$, for methanol while experiment gives 32. By introducing the effect of induced dipoles due to molecular polarizability an $\epsilon(0)=42$ results which is now above experiment. This overshoot is attributed to the fact that some of the collective effects are already included in the enhanced effective dipole moment used in the model [36]. Our results agree with that interpretation, as collective effects should become less important with increasing temperature or decreasing density, so that the differences between the calculated and the experimental dielectric constant would diminish, as indeed is observed.

However, a word of caution on oversimple explanations for such discrepancies is in order. It has to be noticed that not all effects giving rise to such departure from experiment can be ascribed to a somewhat crude modelling of the electrostatics. In fact, the value of $\epsilon(0)$ is also dependent on the ordering state of the sample and the latter obvioulsy arises as a consequence of the combined effects of electrostatics and steric interactions. In consequence, removal of such discrepancies would surely involve more refined models to represent both Coulombic and dispersion interactions. The point merits some pondering about. In fact, it is known from computer studies in molecular crystals that inclusion of detailed interactions between hydrocarbon protons (i.e., CH_3,CH_2) is of fundamental importance for the stability of some lattice structures. The main problem inherent to such fairly detailed representations of the intermolecular interactions concerns computational costs, which would severely limit the time window amenable to be explored by MD simulation means. The point of the dependence of the computed electrostatic properties on details of the *molecular geometry* is glaringly illustrated by the work of Höchtl *et al.* who found that the calculated dielectric constant of liquid water was extremely sensitive to the particular value of the bond angle used in the model, while the strength of the molecular dipole moment had a much smaller influence [37]. This could explain the somewhat puzzling result that even at 500 K, where we expect that the effective dipole moment used in the OPLS model (2.22 D) should give higher values than experiment at those temperatures, the calculated dielectric constant is still below experiment.

C. Time- and frequency-dependent dipole correlation functions

In Fig. 4, the total and single-dipole time autocorrelation functions are shown for several temperatures. As expected, at high temperatures the collective function follows quite closely the curve corresponding to the reorientation of individual dipoles, while with decreasing temperature (or increasing density) cooperative effects are enhanced and both functions depart from each other, being the collective relaxation much more slower.

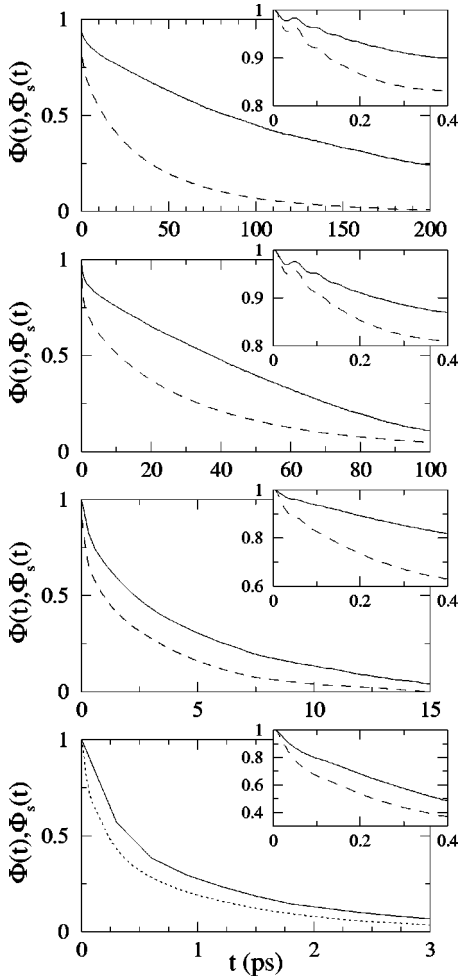

FIG. 4. Total (solid line) and single (dashed line) dipole time autocorrelation functions at several temperatures. The insets show in detail the short time relaxation. From up to down the figures correspond to the following temperatures: 273, 298, 400, and 500 K.

1. Collective dynamics

At very short times, $\Phi(t)$ shows a very rapid decay and an oscillatory behavior with a period of about 0.05 ps. This feature also appears in the self-function and is obviously connected with a very fast movement, apparent also in the atomic velocity autocorrelation function and associated with librational motions of the hydrogen hydroxyl atoms of H-bonded molecules [33]. With increasing temperature these oscillations become blurred because of the diffusive motions, which are gaining importance with respect to vibrations. Beyond 0.5 ps, $\Phi(t)$ can be well fitted by a biexponential function, as found for methanol [36]. Thus, we have fitted the region $0.6<t<50$ ps, where the statistics are good enough to obtain reliable data (see Fig. 2) , to a sum of two exponentials. The relaxation times τ_1^{col} and τ_2^{col}, obtained for each temperature are given in Table I. Although large uncertainties are involved, as can be gauged by comparing the data corresponding to runs B1–B4, the longer two runs at 298 K give times that agree with each other and with those previously reported [33].

Experimentally, three relaxation regions are found in primary alcohols [5], whose origin is still controversial [5,6,39]. These three distinct regions may be described using three spectral distributions with their corresponding relaxation times. At room temperature, Barthel *et al.* [6] report values for the corresponding relaxation times of 163, 8.97, and 1.81 ps; while Kindt and Schmuttenmaer obtain almost the same value for the main relaxation, which is associated with cooperative motions, but much smaller times for the second and third processes 3.3 and 0.22 ps, respectively. They attribute those differences to the limited spectral range used in the previous study [8].

Our results give smaller times for τ_1^{col} than experiment. The same has been found in methanol [36] and, as for the static dielectric constant, the reasons alluded above concerning the somewhat crude molecular model employed should be at the origin of such discrepancy.

In what concerns the characteristic time τ_2^{col} associated with the second relaxation region and evaluated from the fit of $\Phi(t)$, it has to be pointed out that it can only be estimated under large uncertainties. These arise from the small amplitude of the signal as compared to the main relaxation, the presence of more than one spectral component (as will be discussed below), and finally, the large error bars associated with the calculation of this property, as discussed above. Our fitted value for τ_2^{col} is close to the time found by Barthel *et al.* [6] for their third process, which would imply that there exist another intermediate process that is masked by the statistical accuracy of our data. However, from the data of Kindt and Schmuttenmaer one could argue that it corresponds to the second process, which as for the main relaxation is again faster in our model than in real ethanol, while the third process observed by those authors would correspond to the initial fast decay of $\Phi(t)$, which takes place at times of the same order than that found by them. The relationship between the relaxation times obtained from simulation and experiment and their possible physical origin will be treated in more detail below, once the results obtained for single reorientations are presented.

The temperature dependence of the relaxation times is shown in Fig. 5, together with experimental data [4,13] and the corresponding Arrhenius fits (shown as dotted lines). Even if account is made of the limited temperature interval explored, the statistical errors involved and the discrepancies between experiment and simulation, an extrapolation to lower temperatures suggests that the slower process seen in our simulations is at the origin of the primary α relaxation observed in supercooled liquid ethanol, while the fastest one is somewhat related to the secondary relaxation or β process. The apparent activation energy obtained for the main process is about 23 kJ/mol, which is some 5.5 kJ/mol above that found in dielectric measurements [19]. The computer liquid thus shows a dynamics which is faster and harder than experiment. This surely has to do with the model used to represent the intermolecular interactions which leads to an enhancement of the interparticle correlations at short ranges.

The relaxation times obtained from the simulations using the Debye approach—those calculated as integrals over $\Phi(t)$, using the fitted biexponential function to account for the contribution at times longer than 10 ps—follow the same trend as the experimental data [13,40] and qualitatively agree with them, as Fig. 5 clearly shows. Thus, the temperature dependence of the primary relaxation is reasonably well re-

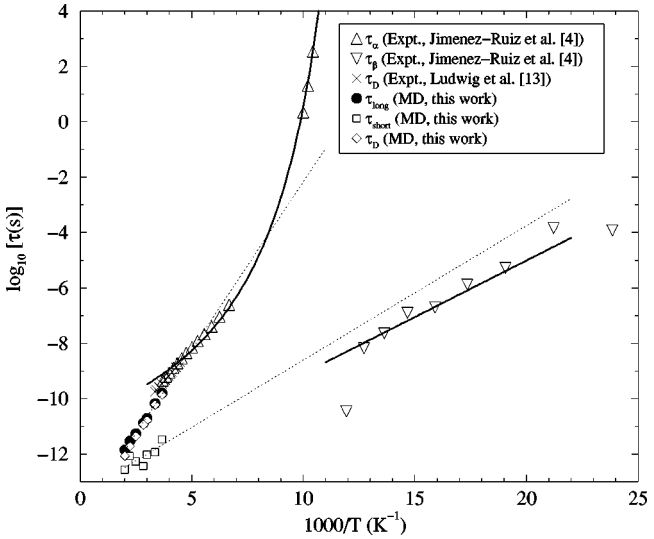

FIG. 5. Dielectric relaxation times. The solid lines correspond to fits to the experimental data [4]. The crosses represent the Debye relaxation times of Refs. [13] and [40]. The circles and the squares correspond to the relaxation times τ_1^{col} and τ_2^{col} obtained from the fit of $\Phi(t)$, respectively, and the diamonds represent the relaxation times obtained integrating $\Phi(t)$.

produced by our simple model.

The second relaxation time τ_2^{col} is obtained less accurately, as evidenced by the scatter of the data shown in Fig. 5. Thus, the statistical accuracy of the parameters derived from the Arrhenius fit to these data is neccessarily low. With such a proviso in mind, we should point out the interesting coincidence between the extrapolated frequencies at temperatures where experiment shows clear β peaks and those actually measured for the β relaxations in the range of temperatures where it becomes well separated from the main relaxation (i.e., basically, below T_g). Such an indication thus suggests that the motions sampled well within the glass phase correspond to those with time scales comparable with τ_2^{col} within the high-temperature liquid.

2. Single-molecule orientational dynamics

The single-dipole correlation function

$$\Phi_s(t)=\langle \boldsymbol{\mu}_i(0)\cdot\boldsymbol{\mu}_i(t)\rangle/\mu^2$$

has been studied in the same way. As it was the case for the collective $\Phi(t)$, a single exponential cannot account for its shape well beyond the initial decay, so again we used two exponentials to fit the data in the same interval as before. The obtained relaxation times τ_1^{self} and τ_2^{self}, are also given in Table I. The same difficulties are experienced here regarding the time range used to fit the curves. While τ_1^{self} is reasonably independent of the chosen lapse of time, τ_2^{self} shows some changes depending on the range employed to fit the curve.

As expected, $\tau_1^{\mathrm{col}} \geqslant \tau_1^{\mathrm{self}}$ for all the explored temperatures and the difference between the two becomes larger as the temperature is decreased. This, which runs in full parallel with the experimental observations, comes as a result of the increasing importance of the coupling of molecular reorientations to the collective degrees of freedom as the temperature decreases which leads to longer times for correlated motions than for those of single molecules. The latter as shown in a recent neutron study [41] are able to reorient at picosecond rates under conditions where the main relaxation time (that of the α peak) already reaches macroscopic times [4]. In other words, at the characteristic temperatures where the supercooled liquid and rotator-phase crystal exist, single-molecule rotations are far less hindered than other motions such as those of collective origin which surely require relatively large rearrangements of neighboring molecules to take place.

One thus expects that the temperature dependence of the single-particle relaxation time τ_1^{self} shows a far milder behavior than their collective counterpart, as indeed is observed. Furthermore, at sufficiently high temperature one also expects that τ_1^{self} should approach a limit where the single-molecule relaxation function could be approximated by the form [42]:

$$\Phi_s(t)\propto\exp\left[-\left(\frac{k_BT}{I_1B_1}+\frac{k_BT}{I_2B_2}+\frac{k_BT}{I_3B_3}\right)t\right], \tag{5}$$

where I_i stand for the principal moments of inertia and B_i for the associated friction constants. Since the ratio of the extreme values for the principal moments of inertia of an isolated ethanol molecule can be as large as 4.2 one may expect to find in such high-temperature limit a clear signature of nonexponential behavior arising from anisotropic molecular reorientations.

As can be seen by the comparison between $\Phi_s(t)$ and $\Phi(t)$ provided in Fig. 4, there are still some clear differences in the shape of the two functions at the highest explored temperature. To allow a direct comparison with the experimental data of Barthel *et al.* [6] we fitted $\Phi_s(t)$ to the sum of two and three exponentials. In doing that we noticed that while the relaxation times corresponding to the α process remained unaffected by the number of fitted decays, the value of τ_2^{self} is then split into two having times of the same order of those given by experiment. The times so obtained are given within parenthesis in Table I.

Above 400 K, we did not get reliable values for relaxation times when employing a third process. Moreover, we could not either fit the collective function to a sum of three exponentials at any temperature. The fact that this could only be done for $\Phi_s(t)$ at the lowest explored temperatures can be rationalized on the basis of (a) a widening of the time scale separation between the three relaxations as the temperature is decreased and (b) the much better statistical accuracy of $\Phi_s(t)$ as compared with its collective counterpart. In other words, the closeness in time scales as temperature raises together with the dominant weigth of the lower-frequency α peak, makes the parameter estimation problem strongly ill conditioned, and thus no reliable values for the smaller times can be derived in this temperature range.

As referred above, a further complication to be taken into account concerns the anisotropic nature of the molecular rotations. This would render inadequate the description of such motions in terms of an unique relaxation time. However, from Eq. (5) it becomes clear that the relevant quantities are the products I_iB_i of moments of inertia and friction terms. As discussed below, a partial compensation of effects seems

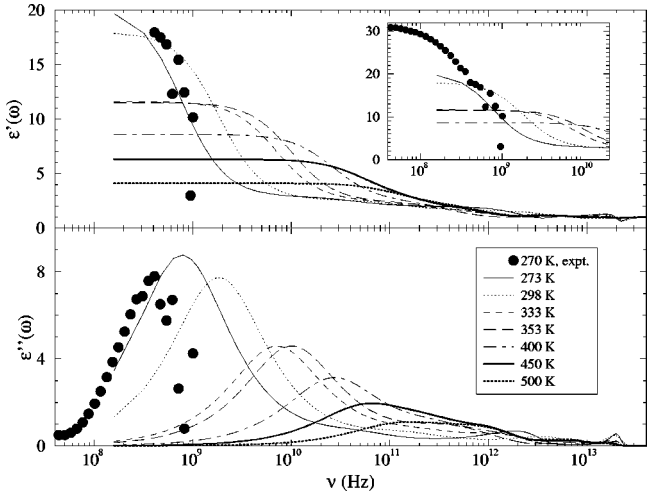

FIG. 6. Real and imaginary parts of the frequency dependent dielectric function at the temperatures studied.

to be in operation since as NMR experiments reveal, the stronger anisotropy occurs at low temperatures.

3. Dielectric relaxation spectrum

The dispersive ϵ' and dissipative ϵ'' parts of the dielectric function as calculated from the relaxation spectra described above are shown in Fig. 6. The spectra have been calculated following Ref. [31] using the fitted relaxation times to evaluate the low-frequency part. At least four different extrema are now revealed in both ϵ' and ϵ''. These appear as dispersion signals in ϵ' and as peaks and shoulders in ϵ''. The latter function shows a strong low-frequency, or α peak, a clear shoulder, and two high-frequency peaks. Taking the 273 K spectra as a reference, one sees the strong α peak centered at about 8×10^{8} Hz, followed by a clear shoulder around 6×10^{10} Hz, a well defined peak at about 2×10^{12} Hz and finally, a narrow feature at a frequency somewhat in excess of 2×10^{13} Hz. The assignment of these features is facilitated by having at our disposal information on the time dependence of $\Phi(t)$. The last peak can thus be unambiguously identified with the high-frequency oscillation seen in both $\Phi_s(t)$ and $\Phi(t)$. Its physical origin is thus ascribed to a high-frequency vibrational motion as referred to above, and its narrow shape is indicative of a rather localized nature. The somewhat broader peak appearing at frequencies about 2×10^{12} Hz shows the characteristics usually ascribed to a β relaxation. Its frequency follows a milder dependence with temperature than that exhibited by the stronger α peak and, as shown in Fig. 5, such dependence would, at temperatures below T_g match that reported by relaxation experiments [4]. While assignment of the lowest frequency peak presents no significant difficulty since it shows the behavior expected for an α-relaxation peak and also has a clear time-domain counterpart, assignment of the shoulder which appears about two frequency decades above it is definitely more involved. Such a feature is also present in the experimental spectrum of many glass-formers and is usually referred to as a ''wing.'' Because of its rather structureless and fairly broad shape it cannot be identified with any definite feature in the time-domain spectra, although its presence together with the ''β peak'' explain the difficulties to describe the time-domain spectra in terms of a sum of exponentials which were commented above.

What, however, gives some hints about its nature is its dependence with temperature. This is revealed, even to the most cursory glance, by following the temperature shifts of such shoulder together with that of the main peak. In doing this one sees that both the α peak and the shoulder follow basically the same temperature dependence while the higher frequency peak shows a milder behavior and the highest peak shows no strong dependence with temperature.

In parallel with the way followed to analyze experimental data [4], both ϵ' and ϵ'' extending up to frequencies covering the α peak and the ''wing'' have been fitted simultaneously using a model function built from two Cole-Davidson distributions. Such a model was able to describe the data very accurately and from there values for two relaxation times specifying the main peak and ''wing'' were derived. In doing so we found that both the temperature dependence of both relaxation times followed Arrhenius behaviors with activation energies of 19.7 and 19.4 kJ/mol, respectively. The main difference between both distributions thus regards the preexponential factors which are now different by two orders of magnitude. As expected, the exponents of both distributions were found to have reached the Debye limit quite closely (i.e., both are basically unit) and the relaxation strengths $\epsilon_0-\epsilon_\infty$ were also found to behave quite differently, that of the main band exhibiting a linear decrease with temperature while that for the ''wing'' shows a scant dependence.

4. Frequency spectra of the single-dipole correlation function

The spectra of $\Phi_s(t)$ have also been evaluated following the same procedure than that employed for its $\Phi(t)$ collective counterpart. Although such transforms are quantities not amenable to experiment they can be interpreted as those describing the projection of all the liquid dynamics into a ''tagged'' molecular dipole and therefore play the same role as the generalized frequency distribution for a monoatomic fluid.

A set of curves showing the dispersive and dissipative parts of the transforms of $\Phi_s(t)$ are depicted in Fig. 7 for and equivalent set of temperatures to that considered for the dielectric function. The most remarkable features exhibited by the aforementioned graphs are the presence of a minimum of five spectral components which show somewhat disparate dependences with temperature. The lowest frequency and most intense feature which appears as a peak at about 4×10^{9} Hz shows a very marked shift towards higher frequencies as the temperature is raised. The same applies to a high-frequency wing which is barely visible below the main peak at the lowest temperature but it is seen as a clear shoulder at 6×10^{10} Hz at intermediate temperatures ($\approx$350 K), as well to a well defined shoulder seen at about 2×10^{11} Hz at the lowest temperature. In contrast the higher-frequency features such as the narrow peak at 2×10^{13} Hz, the shoulder at about 5×10^{12} Hz, the peak at about 2×10^{12} Hz and the intensities within the region $0.3–2\times10^{12}$ Hz experience a rather mellow temperature dependence, showing in all these cases a small frequency softening as the temperature is raised.

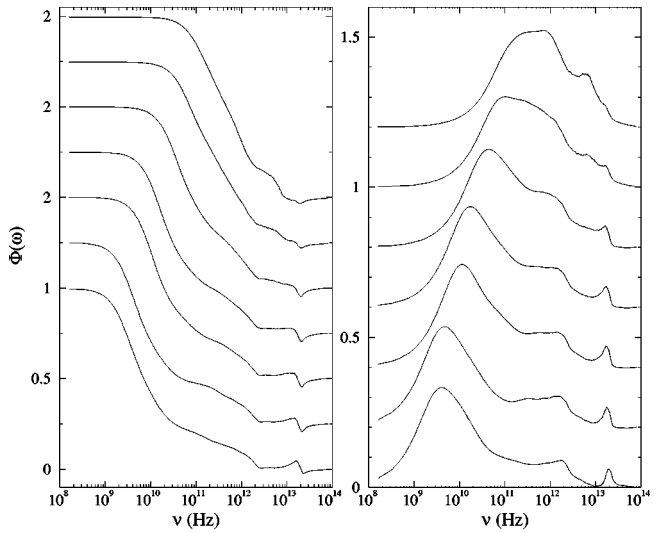

FIG. 7. Real and imaginary parts of the frequency spectrum of the single-dipole autocorrelation function at the temperatures studied.

The behaviors referred in the above paragraph seem indicative of the existence of two relatively well separated frequency domains in the spectrum of $\Phi(t)$ which comprise the region of the α peak including its leading edge (the ''wing'') and the higher-frequency shoulder and the higher-frequency features. Because of the similitude of the temperature dependences it is appealing to consider that motions taking place up to frequencies comprising the main peak, wing and shoulder are of the same nature involving a strong coupling with the macroscopic viscosity whereas those at higher frequencies concern fairly localized motions.

D. Geometry of single-molecule reorientations

We have analyzed the rotational motions of the individual molecules by monitoring the reorientations about directions defined by each of the intramolecular bonds used in our simple model, i.e., CC, CO and OH. None of these coincides with any of the principal axis of inertia and therefore all the calcuated quantities are expected to show some complicated dependence with time. Their behavior at room temperature is shown in Fig. 8 together with that corresponding to the molecular dipole moment vector. The rapid initial decay of the function associated with the CC vector can be attributed to the extra movility provided by the internal torsion, which at room temperature has a very short relaxation time (less than 1 ps), as shown before [21]. This effect would also favor the rotation of the OH vector, but this one is impeded by the hydrogen bonds formed along its direction, as they have to be broken to allow this vector to rotate. Additionally, on the grounds of molecular geometry the rotations around the axis of inertia that imply less rearrangements of neighboring molecules will be favored, so the net result is a combination of the influence of the hydrogen-bond network and steric effects.

Ludwig *et al.* have obtained rotational correlation times for the OH group at several temperatures by means of NMR relaxation experiments [13]. The relaxation times measured by this technique are, in principle, equivalent to the integral

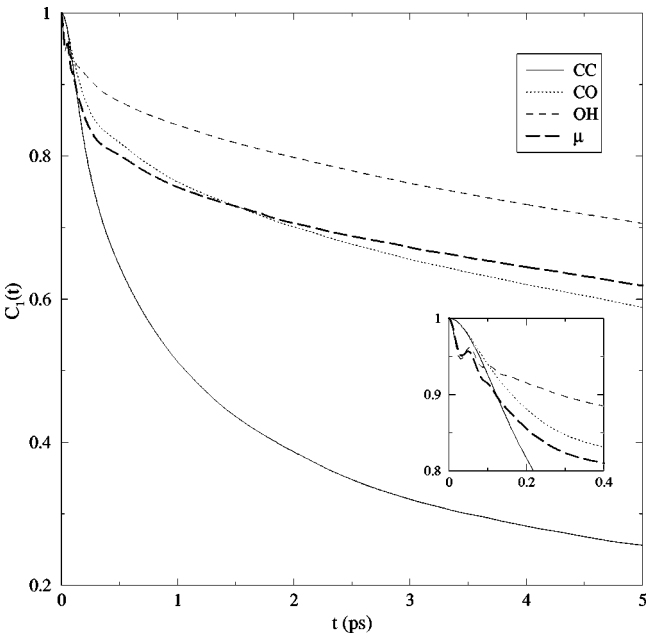

FIG. 8. Reorientational autocorrelation function of the intramolecular vectors at 298 K. The inset shows in detail the short time behavior.

of $C_2^{\mathrm{OH}}(t)$, where $C_2(t)=\langle P_2[\cos\theta(t)]\rangle$, where $P_2(x)$ is the second Legendre polynomial and $\theta(t)$ the angle swept by the appropriate reference vector. We compare the times obtained in such a way with experiment in Fig. 9. We have also plot-

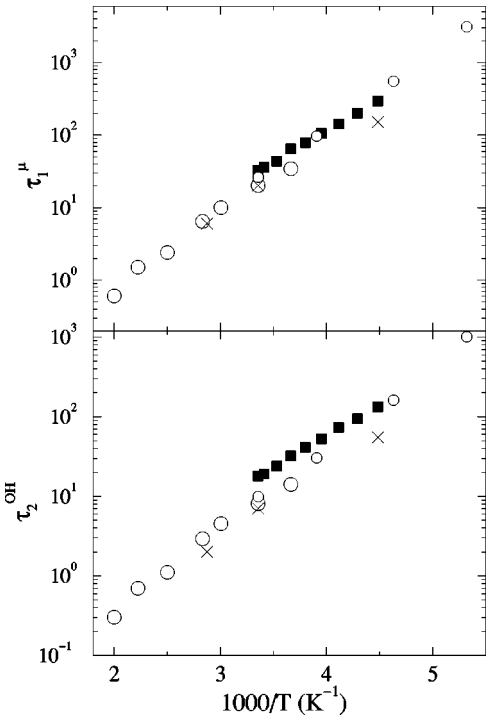

FIG. 9. (Up) Longitudinal dielectric correlation times (see text). The black squares correspond to the experimental data [13] and the big open circles to the present simulations. The small circles correspond to previous results obtained at a pressure of 0.8 kbar [21] and the crosses to simulations done using the Ewald sums [33]. (Down) Rotational correlation times of the OH vector (see text). Symbols as above.

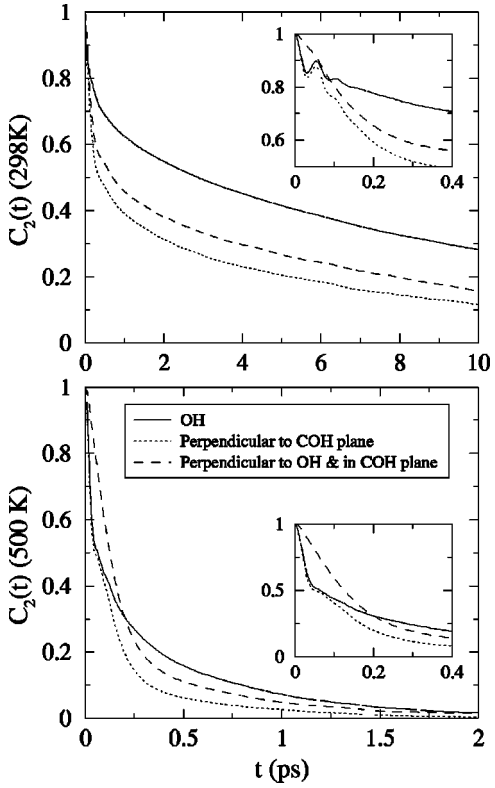

FIG. 10. Reorientational autocorrelation function of the OH vector and two vectors perpendicular to it at 298 (up) and 500 K (down).

ted in that figure the longitudinal dielectric correlation times given by the same authors, which are related to the macroscopic relaxation time τ_D shown before and can be compared with the integral reorientational correlation times of $\Phi_s(t)$. As before, the experimental times are larger than the computed ones and the activation energies evaluated from Arrhenius fits to the reorientational times are also higher than experiment [13] (19 and 20 kJ/mol for the OH and μ reorientations, respectively, instead of 15.0 and 16.2 KJ/mol [13]). However, the general temperature dependence is again quite well reproduced by the simulation.

NMR experiments have also demonstrated the large rotational anisotropy of ethanol [9,10,12]. Thus, together with the behavior of the OH vector we have studied also how two perpendicular vectors to this one reorient: one in the COH plane and the other perpendicular to it. Figure 10 shows the results obtained at two different temperatures. The OH vector presents the slowest relaxation, due perhaps to the formation of H bonds along its direction which, if this was the case, need to be broken in order to allow for their reorientation. The rapid librational motion commented before is apparent in the curves corresponding to the OH vector and the vector perpendicular to the COH plane, while it is absent in the other, giving us some clues about the ''geometry'' of that motion.

Fitting the relaxation times to an Arrhenius law we find that the reorientation about the OH vector has the highest activation energy (19 kJ/mol), while the other two have similar activation energies (≈ 17 kJ/mol), in agreement with experiment, although as before we obtain higher values than those evaluated from NMR data. The temperature dependence of those relaxation times also agree with the experimental finding that rotational anisotropy decreases as the temperature increases [12].

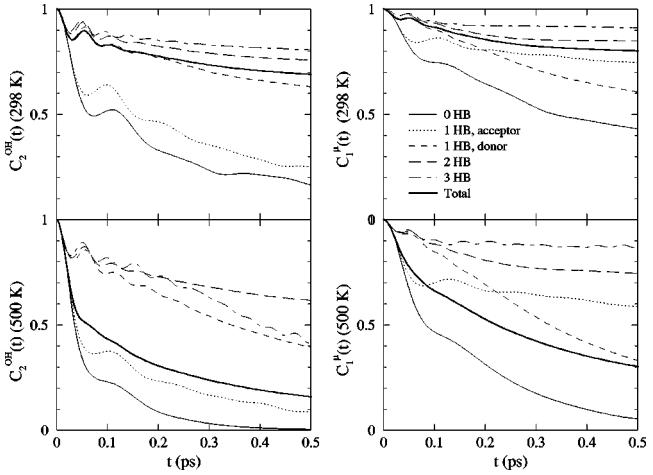

FIG. 11. Reorientational autocorrelation functions of the OH (left) and dipole moment (right) vectors for molecules with different number of H bonds at 298 (up) and 500 K (down).

To study the influence of H bonding we have recalculated those reorientational autocorrelation functions by taking into account the H-bond state of the molecule. To do this, we first determine for a given molecule how many H bonds it has and then calculate the correlation function for a time interval as long as the molecule remains in the same state, i.e., as long as it does not break any H bond or form a new one. The existence of a H bond has been determined using a geometric criterion, i.e., we consider that two ethanol molecules are H bonded if $r(\mathrm{O}\cdots\mathrm{H}) \leqslant 2.6$ Å, $r(\mathrm{O}\cdots\mathrm{O}) \leqslant 3.5$ Å and the angle $(\mathrm{HO}\cdots\mathrm{O}) \leqslant 30°$. For the case of ethanol, both the geometric or the energetic definition of a H bond give very similar results [20]. Figure 11 shows the results corresponding to the OH and dipole moment vectors at the same two temperatures shown in the previous figure. These functions can only be calculated for short time periods, as at the temperatures studied H bonds break and reform rapidly, and their statistical accuracy depends in the average number of molecules belonging to each state.

As expected, free molecules show the faster reorientation and as regards the OH vector, molecules that have only one acceptor HB behave in a very similar way to monomers, as the HB does not hinder its motion in that case. This is not the case for molecules with a single HB but acting as donors, where the OH bond gets ''fixed'' and exhibits a behavior close to that of molecules with two or more HB.

In terms of the dipole moment, molecules with only one donor HB show a very rapid reorientation, even faster than that corresponding to molecules with only one acceptor HB. As when acting as a donor, the O and H atoms are relatively fixed (see the curves corresponding to the OH rotation), this reorientation must be due to rotations around the OH bond that would lead to a displacement of the nearest carbon to the hydroxil group, which also shares some electrostatic charge in our model. The internal degree of freedom of the molecule possibly facilitates this motion. However, it is not clear why the rapid OH rotation of only acceptor molecules does not induce an equally rapid dipole rotation.

The total correlation functions are shown as thick solid lines in Fig. 11. They correspond to a weighted average over all the possible H-bond states, where the weighting factors are the fraction of molecules with a given number of HB's. Thus, at 298 K where 84% of the molecules have two or more HB the total function decays very slowly following the behavior corresponding to ''linked'' molecules. Instead, at 500 K where almost 80% of the molecules are monomers or have only one HB, the decay of the total function is close to that of those ''mobile'' molecules.

An alternative view. While rationalizing the observations in terms of hydrogen-bonding interactions constitutes a frame of reference which is justified in terms of chemical intuition, an alternative view of the dynamics of this exceedingly interesting liquid is provided by a recent study on the details of molecular motions within the rotator-phase crystal [41]. The relevance of such an study for our present purpose stems from the remarkable similitudes in local order between the normal liquid and the cubic bcc phase of the RP crystal. This study using MD and quasielastic neutron scattering as concurrent tools has evidenced the presence of reorientational motions at both picosecond and nanosecond scales within the crystal, while the experimental dielectric relaxation time varies within the 10^{-2}–10^{3} s time range [41]. The most relevant part of such a study concerns the assignment of specific microscopic reorientations to the neutron scattering signals. This is here facilitated by the presence of an underlying cubic lattice for the molecular centers of mass, which bounds the number of possible reorientations down to a manageable number. These are those connecting some 24 different basic orientations which arise in order to compensate for the different crystal site and molecular point group symmetries, and may be viewed as angular excursions from a ''preferred orientation'' given as that where the C—O bond approximately lies on the cube edge and the C—C bond lies on the cube diagonal. As all diagonals and edges are equivalent by symmetry, the molecule would perform dynamical reorientations among the referred 24 orientations. From those, the most probable are the reorientations bringing the C—O bonds from the preferred orientation to all [100] directions of the bcc lattice and the C—C bonds to all [111] directions. Within the cubic crystal these are 90° rotations about an axis a few degrees offset from the C—O bonds (C_4) and 120° rotations around another axis also somewhat offset from the C—C bond (C_3). In either case, one of the bonds is kept invariant whereas in both cases the normal to the C—C—O plane reorients to a new direction. Such motions are there found to be those which can be executed with minimal rearrangements in the orientation of neighboring molecules and occur in a scale of picoseconds. Other rotational motions which would involve larger angular excursions of the OH fragment such are the rotations (C_4') around the [100] directions perpendicular to the C—O bond, the threefold rotations C_3' around the three [111] crystal directions different from that of the C—C bond and the twofold rotations C_2 around the [110] crystal directions, will also occur. Their frequency, however, was found to be significantly smaller than that of the faster reorientations.

In consequence and having in mind the proviso of comparing a system with long-range order in a time-average sense for the molecular centers-of-mass with a liquid, one can understand the very different reorientational properties of the three molecular vectors in the light of the results just referred as a net effect of the packing of neighboring molecules. In any case, further theoretical and experimental studies are required in order to be able to determine unambiguously the role played by steric and electrostatic effects in this or similar systems [43,44].

IV. DISCUSSION AND CONCLUSIONS

The main drawback of the interparticle potential used for the current simulation concerns the reduced values of the static dielectric constant and the dielectric or reorientational correlation times with respect to experiment. Such a discrepancy which is shared by a good number of simulations carried out for similar systems indicates that the model potential gives rise to too fast reorientational dynamics. This shortcoming cannot be solely attributed to the modelling of the electrostatic interactions since steric effects will also play a significant role in driving a dynamics which is faster than in experiment.

The model used is, however, able to reproduce qualitatively the experimental observations as well as the general trends exhibited by the temperature dependence of the parameters characterizing the main spectral bands. At room temperature, the relaxation spectrum ϵ'' shows four well-defined features having associated relaxation times which are in semi-quantitative agreement with those of the three main bands reported by experiment [6,8]. The slowest relaxation time is the parameter better defined. Its collective nature is demonstrated by its temperature dependence which resembles that of the shear viscosity.

As expected, the temperature dependence of the relaxation times follows Arrhenius laws within the whole temperature range. If this behavior is extrapolated to lower temperatures one finds that the simulation should match the primary (α) and secondary (β) relaxations observed in experiments [4]. However, longer simulations should be done at low temperatures in order to check whether this extrapolation is valid and determine how the α relaxation starts to deviate from Arrhenius behavior when approaching the glass transition temperature. Some signs of this incipiently diverging behavior have been found previously when studying some other single-particle properties. However, what hampers further progress in conducting studies in the interesting region of the deeply supercooled liquid, is the fact that the dielectric relaxation times near T_g are far too long (of the order of hundreds of seconds) to be reachable by brute-force computer simulations.

The total dipole autocorrelation function shows a rapid initial decay at times less than 0.5 ps which is followed by a two-exponential decay. The origin of such rapid decay surely has to do with the lowest frequency molecular librations as well as with high-frequency vibrations. On the basis of previous calculations for the glass [4], supercooled liquid, and monoclinic crystal [17], the lowest frequency whole-molecule librations which show a main peak at frequencies about 2 THz where found to be the microscopic entities giving rise to the β relaxation.

As regards the microscopic nature of dynamic processes giving rise to the relaxation bands having frequencies located

between the main α peak and those of microscopic nature (i.e., the β peak and the higher frequency libration), the difficulty of assigning an specific microscopic entity to those arises from the fact that they are located in a frequency range which is in between that dominated by stochatic motions (molecular rotations and translations) and a regime where the liquid short-time dynamics (i.e., vibrations) become dominant. The safest approach is thus to consider the relaxation times characterizing this spectral region as a means to describe the data since such regions of the spectrum surely include different motional contributions having rather similar relaxation times.

In summary, computer simulations carried on moderately sized samples are able to predict the most salient features of the dielectric function. The main limitation to cross over to the regime below T_A seems to be linked to the accuracy with which the relevant autocorrelation functions are evaluated, but not with the system size. In other words, this suggests that the relevant interactions which will give rise to glassy dynamics at lower temperatures are confined down to a few tens of Å. Finally, it has become apparent that a truly microscopic approach is needed to understand in detail the origin of relaxations occurring at higher frequencies than the main α peak. Molecular motions within this range of frequencies should be regarded as arising from an interplay between stochastic (rotational and translational difusion) and vibrational (high-frequency librations) motions which need to be modelled in detail.

ACKNOWLEDGMENTS

The authors acknowledge the financial support of DGICYT/Spain through Grant No. No. PB95-0072-C03. M.A.G. thanks the Institut Laue-Langevin for the concession of a CFR contract. We thank N. G. Almarza for stimulating discussions. The CSC of the Universidad Complutense de Madrid is acknowledged for granting us access to computing resources.

[1] S. Brawer, *Relaxation in Viscous Liquids and Glasses* (The American Ceramic Society, Columbus Ohio, 1985).

[2] E. Donth, *Relaxation and Thermodynamics in Polymers* (Akademie Verlag, Berlin, 1992); see also D. Kirkpatrick and D. Thirumalai, Phys. Rev. A **40**, 1045 (1989).

[3] E. W. Fischer, Physica A **201**, 183 (1993); A. Schönhals *et al.*, Phys. Rev. Lett. **70**, 3459 (1993).

[4] M. A. Miller, M. Jiménez-Ruiz, and F. J. Bermejo, Phys. Rev. B **57**, 13 977 (1998); M. Jiménez-Ruiz, M. A. González, F. J. Bermejo, M. A. Miller, N. O. Birge, I. Cendoya, and A. Alegría, *ibid.* **59**, 9155 (1999).

[5] S. K. Garg and C. P. Smyth, J. Phys. Chem. **69**, 1294 (1965).

[6] J. Barthel, K. Bachhuber, R. Buchner, and H. Hetzenauer, Chem. Phys. Lett. **165**, 369 (1990); W. R. Fawcet, *ibid.* **199**, 153 (1992).

[7] F. Stickel, E. W. Fischer, and R. Richert, J. Chem. Phys. **104**, 2043 (1996).

[8] J. T. Kindt and C. A. Schmuttenmaer, J. Phys. Chem. **100**, 10 373 (1996).

[9] H. Versmold, Ber. Bunsenges. Phys. Chem. **78**, 1318 (1974).

[10] B. M. Fung and T. W. McGaughy, J. Chem. Phys. **65**, 2970 (1976).

[11] T. Eguchi, G. Soda, and H. Chihara, Mol. Phys. **40**, 681 (1980).

[12] Z. Zheng, C. L. Mayne, and D. M. Grant, J. Magn. Reson. Sec. A **103**, 268 (1993).

[13] R. Ludwig and M. D. Zeidler, Mol. Phys. **82**, 313 (1994); R. Ludwig, M. D. Zeidler, and T. C. Farrar, Z. Phys. Chem. (Leipzig) **189**, 19 (1995).

[14] M. P. Janelli, S. Magazú, P. Migliardo, F. Aliotta, and E. Tettamanti, J. Phys.: Condens. Matter **8**, 8157 (1996).

[15] A. Srinivasan, F. J. Bermejo, A. de Andrés, J. Dawidowski; J. Zúñiga, and A. Criado, Phys. Rev. B **53**, 8172 (1996); R. Fayos, F. J. Bermejo, J. Dawidowski, H. E. Fischer, and M. A. González, Phys. Rev. Lett. **77**, 3823 (1996); F. J. Bermejo, A. Criado, R. Fayos, R. Fernández-Perea, H. E. Fischer, E. Suard, A. Guelylah, and J. Zúñiga, Phys. Rev. B **56**, 11 536 (1997).

[16] M. A. Ramos, S. Vieira, F. J. Bermejo, J. Dawidowski, H. E. Fischer, H. Schober, M. A. González, C. K. Loong, and D. L. Price, Phys. Rev. Lett. **78**, 82 (1997).

[17] C. Talón, M. A. Ramos, S. Vieira, G. J. Cuello, F. J. Bermejo, A. Criado, M. L. Senent, S. M. Bennington, H. E. Fischer, and H. Schober, Phys. Rev. B **58**, 745 (1998).

[18] O. Haida, H. Suga, and S. Seki, J. Chem. Thermodyn. **9**, 1133 (1977).

[19] S. Benkhof, A. Kudlik, T. Blochowicz, and E. Rössler, J. Phys.: Condens. Matter **10**, 8155 (1998).

[20] M. A. González, E. Enciso, F. J. Bermejo, and M. Bée, J. Chem. Phys. **110**, 8045 (1999).

[21] M. A. González, E. Enciso, F. J. Bermejo, and M. Bée, Phys. Rev. B (to be published).

[22] W. L. Jorgensen, J. Phys. Chem. **90**, 1276 (1986).

[23] B. D. Smith and R. Srivastava, *Thermodynamic Data for Pure Compounds* (Elsevier, Amsterdam, 1985).

[24] M. P. Allen and D. J. Tildesley, *Computer Simulation of Liquids* (Oxford University Press, Oxford, 1987).

[25] J. P. Ryckaert, Mol. Phys. **55**, 549 (1985).

[26] D. J. Adams, E. M. Adams, and G. J. Hills, Mol. Phys. **38**, 387 (1979).

[27] J. Alonso, F. J. Bermejo, M. García-Hernández, J. L. Martínez, W. S. Howells, and A. Criado, J. Chem. Phys. **96**, 7696 (1992).

[28] O. Steinhauser, Mol. Phys. **45**, 335 (1982).

[29] L. Perera, U. Essmana, and M. L. Berkowitz, J. Chem. Phys. **102**, 450 (1995).

[30] P. H. Hünenberger and W. F. van Gunsteren, J. Chem. Phys. **108**, 6117 (1998).

[31] M. Neumann, Mol. Phys. **50**, 841 (1983); M. Neumann, O. Steinhauser, and G. S. Pawley, *ibid.* **52**, 97 (1984).

[32] The errors in the static dielectric constant were calculated from the error in $\langle \boldsymbol{M}^2 \rangle$, which was evaluated using the appropriate expression for the variance of correlated data following M. Bishop and S. Frinks, J. Chem. Phys. **87**, 3675 (1987).

[33] L. Saiz, J. A. Padró, and E. Gukrdia, J. Phys. Chem. B **101**, 78 (1997); L. Saiz, Ph. D. Thesis, University of Barcelona, 1998.

[34] D. van der Spoel, P. J. van Maaren, and J. C. Berendsen, J. Chem. Phys. **108**, 10 220 (1998).
[35] T. Fonseca and B. M. Ladanyi, J. Chem. Phys. **93**, 8148 (1990).
[36] M. S. Skaf, T. Fonseca, and B. Ladanyi, J. Chem. Phys. **98**, 8929 (1993).
[37] P. Höchtl, S. Boresch, W. Bitomsky, and O. Steinhauser, J. Chem. Phys. **109**, 4927 (1998).
[38] P. Jedlovszky and J. Richardi, J. Chem. Phys. **110**, 8019 (1999).
[39] G. Salvetti, in *Hydrogen-bonded Liquids*, edited by J. C. Dore and J. Teixeira, Vol. 329 of *NATO Advanced Studies Institute*, Series C (Reidel, Dordrecht, 1991).
[40] S.-G. Su and J. D. Simon, J. Chem. Phys. **89**, 908 (1988).
[41] M. Jimenez-Ruiz, A. Criado, F. J. Bermejo, G. J. Cuello, F. R. Trouw, R. Fernández-Perea, H. Löwen, C. Cabrillo, and H. E. Fischer, Phys. Rev. Lett. **83**, 2757 (1999).
[42] J. McConell, *The Theory of Nuclear Magnetic Relaxation in Liquids* (Cambridge University Press, Cambridge, 1987), p. 183.
[43] A. Criado, M. Jiménez-Ruiz, C. Cabrillo, F. J. Bermejo, R. Fernández-Perea, H. E. Fischer, and F. R. Trouw, Phys. Rev. B (to be published).
[44] M. A. González *et al.* (unpublished).
[45] D. Bertolini, M. Cassettari, and G. Salvetti, J. Chem. Phys. **78**, 365 (1983).
[46] W. Dannhauser and L. W. Bahe, J. Chem. Phys. **40**, 3058 (1964).